TÜBİTAK

Structural and magnetic properties of Mg$_{0.8-x}$M$_{0.2}$Ni$_x$Fe$_2$O$_4$ (M = Zn, Mn) ferrite powders

Mansour AL-HAJ

Physics Department, Mutah University, Mutah-JORDAN
e-mail: mansour@mutah.edu.jo

Abstract

Structural and magnetic properties of Mg$_{0.8-x}$M$_{0.2}$Ni$_x$Fe$_2$O$_4$ (M = Zn, Mn; x = 0, 0.2, 0.4, 0.6, 0.8) ferrite powders, prepared by solid state reaction method, were studied. The variations of lattice parameter, X-ray density, crystallite size, saturation magnetization, effective number of Bohr magneton, and coercivity with Ni content were investigated. The role of grain size was found to be crucial in the behavior of coercivity.

Key Words: Ferrites, lattice parameter, crystallite size, saturation magnetization.

1. Introduction

Polycrystalline spinel ferrites have the general chemical formula MFe$_2$O$_4$, where M is a doubly ionized metal ion. The M^{2+} ions can occupy two types of sites: tetrahedral (A) sites, where each M^{2+} ion is surrounded by four oxygen ions, and octahedral (B) sites, where each M^{2+} ion is surrounded by six oxygen ions. The field of ferrites is very broad due to their interesting properties and diverse applications. Here we present some of the results reported by other workers and are related to our work.

The substitution of Zn in the Ni$_{1-x}$Zn$_x$Fe$_2$O$_4$ ferrite was found to produce appreciable changes in its structural, electrical, magnetic, and density related properties [1, 2]. It was found that the electrical resistivity increases with increasing Mn content in NiZn ferrites [3]. Also, Mn substitution was found to enhance the densification in such materials [4]. The addition of Mn was found to influence the magnetic behavior of NiCuZn ferrites by influencing the microstructure [5]. A significant increase in initial permeability of NiCuZn ferrites was found with the substitution of a small fraction of La for Fe [6]. A similar behavior was reported for the same materials with MoO$_3$ and WO$_3$ additives [7]. The combination of MnZn and NiZn ferrites was found to improve the magnetic properties compared with the individual ones [8]. An improvement in the magnetic properties was found when 0.01 mol of B$_2$O$_3$ was added to NiZn ferrites [9]. The increase in Sm concentration

in NiZn ferrites resulted in the production of powders with good nanometric characteristics [10]. The magnetic behavior of RE-substituted NiMn ferrites indicated that RE ions cannot enter into the ferrite lattice totally, but some reside at the grain boundaries [11]. It was observed that grain size decreases as the Al content increases in $NiFe_{2-x}Al_xO_4$ ferrites [12]. Ball milling of MgZn ferrites up to 25 h was found to lead to the transformation of inverse spinel to normal spinel [13]. The magnetic properties of La-substituted ZnCuCr ferrites were found to be strongly affected by La content [14].

In this work, we investigate the structural and magnetic properties of $Mg_{0.8-x}M_{0.2}Ni_xFe_2O_4$ (M = Zn, Mn) ferrites, where $x = 0$, 0.2, 0.4, 0.6, and 0.8, since these properties are sensitive to ion substitution. For brevity, we refer to the first series of ferrites by the Zn samples, and to the second series by the Mn samples.

2.   Experimental

The samples were prepared by solid state reaction method. Powders of MgO (98%), ZnO (99%), NiO (99%), MnO (99.99%), and Fe_2O_3 (98.5%) were weighed, mixed, and ground in an agate mortar and pestle. The mixtures were then calcined at 1100 ^oC in a Carbolite furnace for 9 h. After calcination, each sample was slowly cooled to room temperature, ground, and calcined again at 1100 ^oC for 9 h. After the second calcination, each sample was ground to get a neat homogeneous powder. The X-ray diffraction (XRD) patterns were taken using a Seifert 3003 TT diffractometer operating at 40 kV and 40 mA employing a Cu target. The instrument was calibrated using a standard Si powder. The magnetic measurements were made on samples of equal mass using a 9600 LDJ vibrating sample magnetometer, which was calibrated using a Ni standard.

3.   Results and discussion

Figures 1 and 2 show the XRD patterns for selected Zn and Mn samples. The formation of the single spinel phase is confirmed in all samples. No other phases were identified in each XRD pattern.
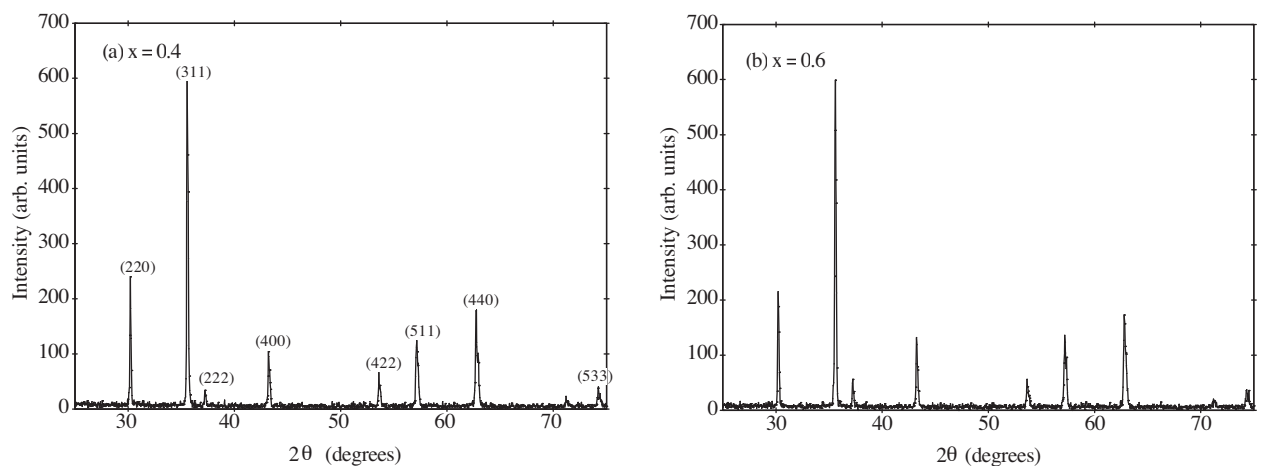

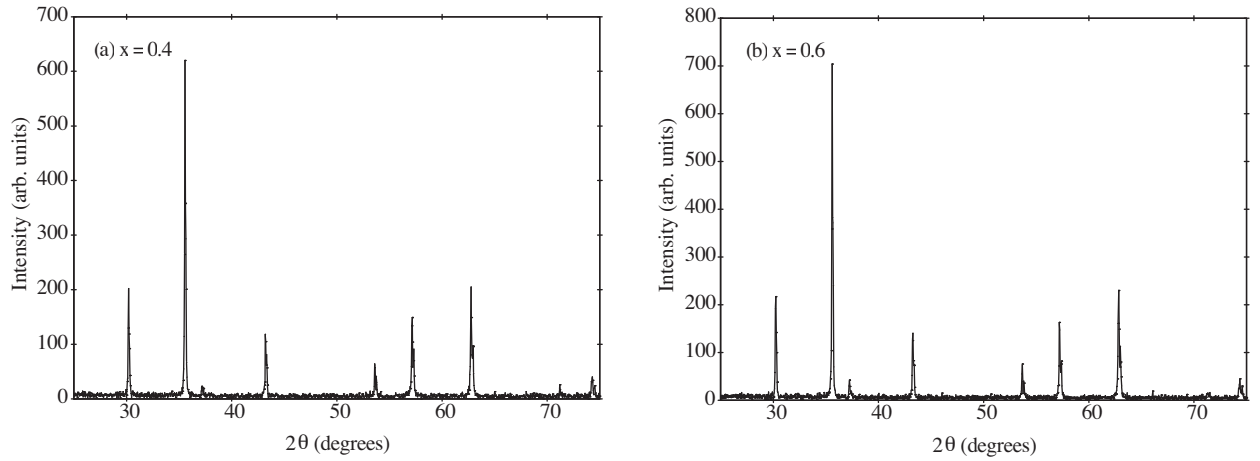**Figure 1.** The XRD patterns for selected Zn samples.

Figure 2. The XRD patterns for selected Mn samples.

The lattice parameter a was calculated using the equation

$$a = d \sqrt{h^2 + k^2 + l^2}, \tag{1}$$

where d is the lattice plane separation and h, k, l are Miller indices. The lattice parameter was calculated employing the strong (311) peak. The lattice parameter a as a function of x is shown in Figure 3 for the Zn and Mn samples (both the calculated values and the fitting lines are shown). For both samples we see that a decreases as x is increased. It is known that Ni^{2+} ions in any ferrite system occupy the octahedral sites, and Mg^{2+} ions have strong preference to occupy these sites [15]. The decrease in a is expected because Mg^{2+} ions in octahedral sites are being replaced by Ni^{2+}, which has a lower radius (the radius of Mg^{2+} in an octahedral site is 0.72 Å, while that of Ni^{2+} in an octahedral site is 0.69 Å [16]). It should be mentioned that the deviation from the line (the ideal linear variation would result if complete substitution of ions were taking place in the ferrite lattice) is larger for the Zn sample than for the Mn sample. This is due to the large tendency of the Zn^{2+} ions to volatilize in air during the calcination process, which leads to a slight change in the stoichiometry of the sample.
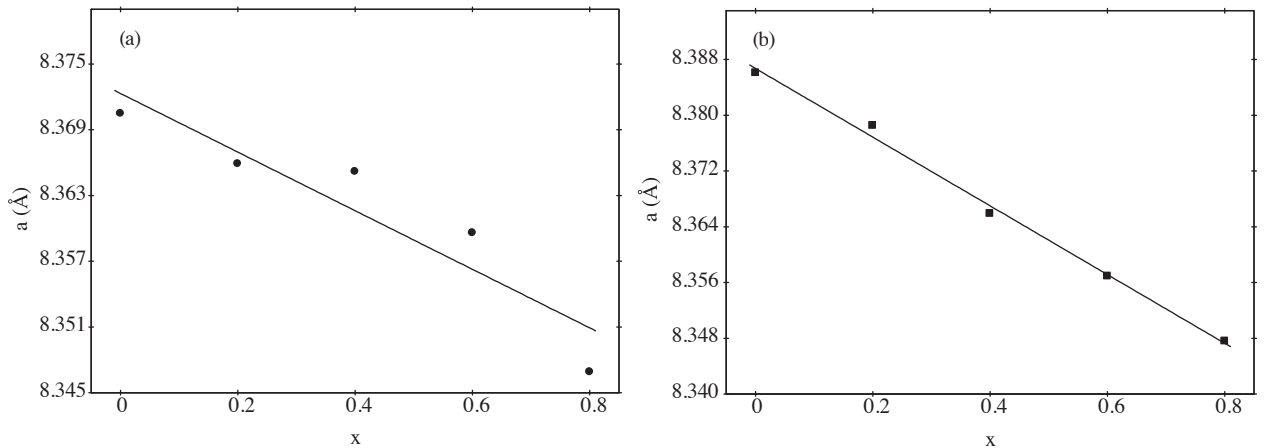

Figure 3. Dependence of the lattice parameter a on x for (a) the Zn and (b) the Mn samples.

The X-ray density (the theoretical density) ρ_X was calculated using the equation

$$\rho_X = \frac{8\,M}{N_A\,a^3},\tag{2}$$

where M is the molar mass of the ferrite, a is the lattice parameter, and N_A is Avogadro's number. The dependence of ρ_X on x for the Zn and Mn samples is shown in Figure 4. It is seen that ρ_X increases linearly with x, since Mg^{2+} ions in octahedral sites are replaced by Ni^{2+} ions, which have a greater mass, and at the same time, the volume of the conventional unit cell is decreasing as x is increased. Further, it is noticed that ρ_X is greater for Zn samples than Mn samples. This is because the mass of Zn^{2+} is greater than Mn^{2+} and, as revealed by the fitting lines in Figure 3, the volume of the conventional cubic unit cell is nearly the same for two corresponding samples, so ρ_X is greater for Zn ferrites.
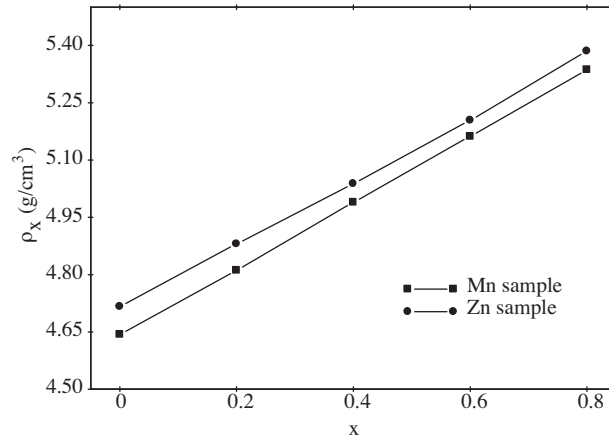

Figure 4. Dependence of the X-ray density ρ_X on x for the Zn and Mn samples.

The average crystallite size D was calculated using the Scherrer equation

$$D = \frac{0.9\,\lambda}{\gamma\,\cos\theta},\tag{3}$$

where λ is the wavelength of the Cu K_α X rays (1.5406 Å), γ is the full-width at half-maximum (FWHM) of the (311) peak in radians, and θ is the Bragg's angle. The variation of D with x for the Zn and Mn samples is shown in Figure 5. The average crystallite size shows a slow decrease with x for the Zn samples. This is consistent with the decrease of the lattice parameter (Figure 3a). The general trend of D for the Mn samples in the range $0 \leq x \leq 0.6$, despite the fluctuations at $x = 0.2$ and 0.4, is to decrease with x. At $x = 0.6$ and 0.8, D has the same value. The fluctuations in the D values at $x = 0.2$ and 0.4 are probably due to the difficulty in keeping the same experimental conditions during sample preparation. Further, it is observed that D is greater for Mn samples than the corresponding Zn samples. This is due to the important role played by Mn^{2+} ions in accelerating crystallite growth and in enhancing densification [4]. The lowest D value obtained (about 50 nm for Zn samples) and the constant value of D at $x = 0.6$ and 0.8 for Mn samples are consequences of the limitation of the solid state synthesis method. Very fine crystallites can be obtained by synthesis methods such as high-energy milling [17] and co-precipitation [18]. We would like to mention that grain size and crystallite

size are not necessarily equal (an example is Sm-substituted NiCuZn ferrites [19]). It happens that very fine particles tend to agglomerate to form large grains [4]. In our study, the crystallite size was used as an indicator for grain size.

All studied samples are soft ferrimagnetic at room temperature. This is evident from the hysteresis loops, which are shown in Figure 6 for selected Zn and Mn samples.
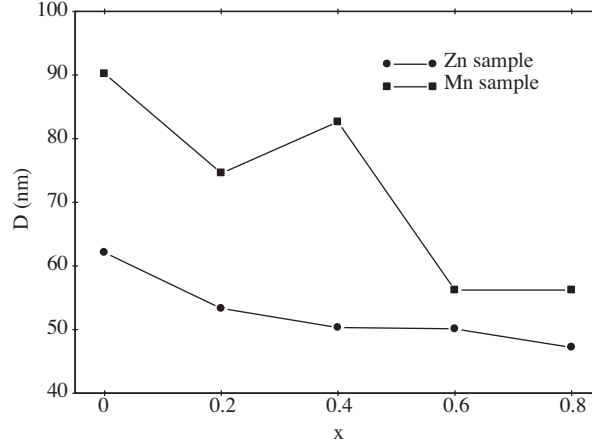

Figure 5. Dependence of the average crystallite size D on x for the Zn and Mn samples.
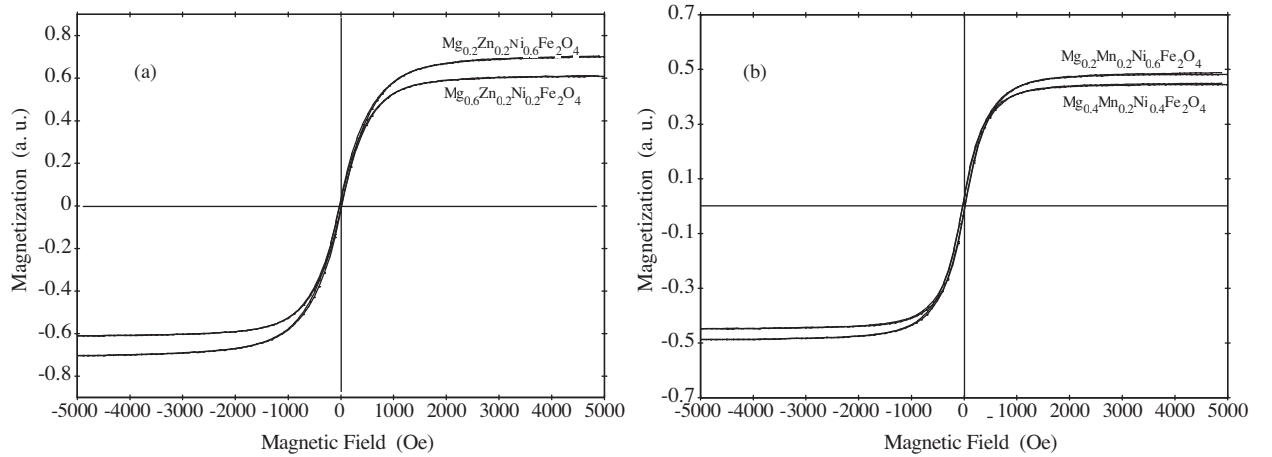

Figure 6. The hysteresis loops for selected (a) Zn and (b) Mn samples.

The saturation magnetization M_s is found to increase with x for both samples, as shown in Figure 7. Such a behavior is expected because the net magnetization of the ferrite lattice is the difference between the contribution from the magnetic ions in octahedral sites and the contribution from those in tetrahedral sites. Since nonmagnetic Mg^{2+} ions in octahedral sites are replaced by magnetic Ni^{2+} ions, the contribution to magnetization from the ions in the octahedral sites increases, with no change in the contribution from magnetic ions in the tetrahedral sites. Consequently, the net magnetization increases. In addition, we see from the figure that the M_s values for the Mn samples are smaller than those for the Zn samples. This is because the magnetic Mn^{2+} ions are replacing nonmagnetic Zn^{2+} ions located in the tetrahedral sites. Consequently, the contribution to magnetization from these ions increases and the net magnetization therefore decreases.
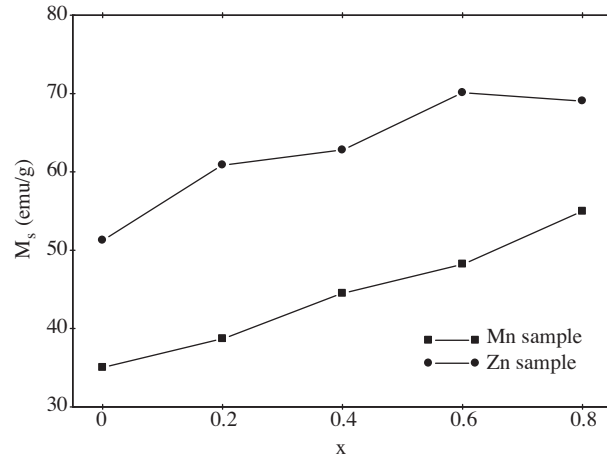
189

Figure 7. Dependence of the saturation magnetization M_s on x for the Zn and Mn samples.

The effective number of Bohr magneton n_{eff} was calculated using the equation

$$n_{eff} = \frac{M \, M_s}{9.27 \, \times \, 10^{-21} \, N_A},\tag{4}$$

where M is the molar mass and N_A is Avogadro's number. The calculated values are tabulated in Table and are in very good agreement with values obtained for other related ferrites [20, 21].

Table. The effective number of Bohr magneton for Zn and Mn samples

x	n_{eff} for Zn samples	n_{eff} for Mn samples
0	1.91	1.29
0.2	2.35	1.48
0.4	2.50	1.75
0.6	2.87	1.96
0.8	2.92	2.30

The variation of coercivity H_c with x for both samples is shown in Figure 8. The coercivity of spinel ferrites is known to be dependent on such factors as grain size, porosity, and microstrains, as we reported in our previous work [15, 22] and as reported by many other workers. It is seen from Figure 8 that H_c increases with x for the Zn samples. Such a behavior is consistent with the decrease in crystallite size (and hence in grain size), because decreasing the grain size increases the interaction between the domain walls and the grain boundaries, leading to an increase in H_c. For the Mn samples, the coercivity increases at $x = 0.2$ and then decreases (we notice from Figure 5 that D decreases at $x = 0.2$). Except for the anomaly at $x = 0.6$ and 0.8 for the Mn samples, we can say that H_c of both samples is governed by grain size.

190

Figure 8. Dependence of the coercivity H_c on x for the Zn and Mn samples.

4. Conclusions

(1) The spinel phase was confirmed in all samples.

(2) The lattice parameter decreases and the X-ray density increases as x is increased in the two ferrite systems.

(3) The crystallite size for the Zn samples decreases slowly as x is increased, while for the Mn samples, it remains constant at $x = 0.6$ and 0.8.

(4) The saturation magnetization increases with x in the two ferrite systems.

(5) The grain size plays an important role in affecting the behavior of H_c in the two ferrite systems.

References

[1] M. Ajmal and A. Maqsood, *Mater. Sci. Eng. B*, **139**, (2007), 164.

[2] I. Gul, W. Ahmed and A. Maqsood, *J. Magn. Magn. Mater.*, **320**, (2008), 270.

[3] A. Sattar, H. El-Sayed, and K. El-Shokrofy, M. El-Tabey, *J. Mater. Sci.*, **42**, (2007), 149.

[4] A. Bueno, M. Gregori, and M. Nbrega, *Mater. Chem. Phys.*, **105**, (2007), 229.

[5] V. Tsakaloudi, E. Eleftheriou, M. Stoukides, and V. Zaspalis, *J. Magn. Magn. Mater.*, **318**, (2007), 58.

[6] P. Roy and J. Bera, *Mater. Res. Bul.*, **42**, (2007), 77.

[7] H. Su, H. Zhang, and X. Tang, Y. Jing, *Mater. Chem. Phys.*, **102**, (2007), 271.

[8] A. Verma and R. Chatterjee, *J. Magn. Magn. Mater.*, **306**, (2006), 313.

[9] B. Yuksel, S. Kirtay, T. Ozkan, E. Acikalin, and H. Erkalfa, *J. Magn. Magn. Mater.*, **320**, (2008), 714.

[10] A. Costa, A. Diniz, A. de Melo, R. Kiminami, D. Cornejo, A. Costa, and L. Gama, *J. Magn. Magn. Mater.*, **320**, (2008), 742.

[11] L. Zhao, H. Yang, L. Yu, Y. Cui, X. Zhao, and S. Feng, *J. Mater. Sci.*, **42**, (2007), 686.

[12] A. Raghavender, D. Pajic, K. Zadro, T. Milekovic, P. Rao, K. Jadhav, and D. Ravinder, *J. Magn. Magn. Mater.*, **316**, (2007), 1.

[13] H. Dutta, M. Sinha, Y. Lee, and S. Pradhan, *Mater. Chem. Phys.*, **105**, (2007), 31.

[14] X. Zhou, J. Jiang, L. Li, and F. Xu, *J. Magn. Magn. Mater.*, **314**, (2007), 7.

[15] M. Al-Haj, *phys. stat. sol. (a)*, **203**, (2006), 343.

[16] C. Giacovazzo (editor), *Fundamentals of Crystallography*, (Oxford University Press, UK, 1992), p. 420.

[17] M. Isfahani, M. Myndyk, D. Menzel, A. Feldhoff, J. Amighian, and V. Šepelák, *J. Magn. Magn. Mater.*, **321**, (2009), 152.

[18] P. Hankare, V. Vader, N. Patil, S. Jadhav, U. Sankpal, M. Kadam, B. Chougule, and N. Gajbhiye, *Mater. Chem. Phys.*, **113**, (2009), 233.

[19] P. Roy and J. Bera, *J. Magn. Magn. Mater.*, **321**, (2009), 247.

[20] A. Akther Hossain, T. Biswas, S. Mahmud, T. Yanagida, H. Tanaka, and T. Kawai, *Mater. Chem. Phys.*, **113**, (2009), 172.

[21] A. Akther Hossain, T. Biswas, S. Mahmud, T. Yanagida, H. Tanaka, and T. Kawai, *J. Magn. Magn. Mater.*, **321**, (2009), 81.

[22] M. Al-Haj, *J. Magn. Magn. Mater.*, **311**, (2007), 517.